

Production of Stop, Sbottom, and Stau at LEP2

A. Bartl¹, H. Eberl²,
S. Kraml², W. Majerotto², W. Porod¹

(1) *Institut für theoretische Physik, Univ. Vienna, Austria*
(2) *Institut für Hochenergiephysik (HEPHY), Vienna, Austria*

Abstract

We present a comprehensive study of pair production and decay of stops, sbottoms, and staus in e^+e^- annihilation at LEP2. We give numerical predictions within the Minimal Supersymmetric Standard Model for cross sections and decay rates, and discuss the important signatures. In the case of stau production we also study the polarization of the τ in the decays $\tilde{\tau}_1 \rightarrow \tau\tilde{\chi}_{1,2}^0$.

1 Introduction

Supersymmetry (SUSY) [1] requires the existence of two scalar partners \tilde{q}_L and \tilde{q}_R (squarks) for every quark corresponding to its two helicity states. For the same reason every lepton ℓ has as supersymmetric partners the sleptons $\tilde{\ell}_L$ and $\tilde{\ell}_R$. Whereas in the case of the first and second generation the \tilde{q}_L , \tilde{q}_R and $\tilde{\ell}_L$, $\tilde{\ell}_R$ states are to a good approximation also the mass eigenstates, this is not expected for the third generation. Quite generally, \tilde{q}_L and \tilde{q}_R ($\tilde{\ell}_L$ and $\tilde{\ell}_R$) mix, the size of the mixing being proportional to the mass of the quark q (lepton ℓ). Thus it may be that one of the mass eigenstates of the stops, \tilde{t}_1 , is the lightest squark. It could even be possible that it is the lightest visible SUSY particle. If the parameter $\tan\beta$, which also enters the mixing, is large ($\tan\beta \gtrsim 10$), also the sbottom \tilde{b}_1 or the stau $\tilde{\tau}_1$ can be relatively light. Therefore, it is interesting to study stop, sbottom, and stau production in the energy range of LEP2, that is $m_Z \leq \sqrt{s} \leq 192.5$ GeV. The present experimental bound from LEP1 for the masses of charged supersymmetric particles is $\tilde{m} \gtrsim 45$ GeV [2, 3]. Stronger limits for the stop mass, up to 55 GeV, are reported from LEP at $\sqrt{s} = 130 - 140$ GeV [4]. The $D\emptyset$ experiment at FNAL obtained additional mass bounds for the stop [5, 3] excluding the mass range $40 \text{ GeV} \lesssim m_{\tilde{t}_1} \lesssim 100$ GeV if the mass difference $(m_{\tilde{t}_1} - m_{\tilde{\chi}_1^0}) \gtrsim 30$ GeV, where the neutralino $\tilde{\chi}_1^0$ is the lightest supersymmetric particle (LSP).

Here we shall calculate the production rates for $e^+e^- \rightarrow \tilde{t}_1 \bar{\tilde{t}}_1$, $e^+e^- \rightarrow \tilde{b}_1 \bar{\tilde{b}}_1$, and $e^+e^- \rightarrow \tilde{\tau}_1 \bar{\tilde{\tau}}_1$ in the whole accessible mass range of LEP2 as a function of the mixing angle. SUSY-QCD corrections as well as initial state radiation (ISR) will be included. We also discuss in detail the decay patterns of these particles. The phenomenology of the decays of \tilde{t} , \tilde{b} , and $\tilde{\tau}$ is different from that of the other squarks and sleptons due to their non-negligible Yukawa couplings.

The framework of our calculations is the Minimal Supersymmetric Standard Model (MSSM) [1]. The parameters which determine the phenomenology of stops, sbottoms, and staus are M , M' , the soft-breaking SU(2) and U(1) gaugino masses, μ , the higgsino mass parameter, $\tan\beta = v_2/v_1$, where v_1 and v_2 are the vacuum expectation values of the two Higgs doublets, m_A , the mass of the pseudoscalar Higgs boson A^0 , and $M_{\tilde{F}}$ ($\tilde{F} = \tilde{Q}, \tilde{U}, \tilde{D}, \tilde{L}, \tilde{E}$) and A_f ($f = t, b, \tau$), the soft-breaking parameters which enter the mass matrices of the stops, sbottoms, and staus.

We shall use the GUT relations $M' = \frac{5}{3} M \tan^2 \theta_W \sim 0.5M$ and $m_{\tilde{g}} = \frac{\alpha_s}{\alpha_w} M \sin^2 \theta_W \sim 0.3M$, where $m_{\tilde{g}}$ is the gluino mass.

In the energy range of LEP2 the most important decay modes of \tilde{t}_1 , \tilde{b}_1 , and $\tilde{\tau}_1$ are $\tilde{t}_1 \rightarrow c \tilde{\chi}_1^0$, $b \tilde{\chi}_1^+$, $\tilde{b}_1 \rightarrow b \tilde{\chi}_1^0$, $b \tilde{\chi}_2^0$, and $\tilde{\tau}_1 \rightarrow \tau \tilde{\chi}_{1,2}^0$, $\nu_\tau \tilde{\chi}_1^-$ (assuming $m_{\tilde{\tau}_1} < m_{\tilde{\nu}, \tilde{\ell}}$). Here $\tilde{\chi}_1^\pm$ is the lighter of the two charginos present in the MSSM and $\tilde{\chi}_1^0$ is the lightest of the four neutralinos (with $m_{\tilde{\chi}_1^0} < m_{\tilde{\chi}_2^0} < m_{\tilde{\chi}_3^0} < m_{\tilde{\chi}_4^0}$). It is important to note that the masses and couplings of the charginos and neutralinos only depend on M , μ , and $\tan \beta$.

In the next section we present the formulae for the sfermion mixing, the production cross sections and the decays of \tilde{t}_1 , \tilde{b}_1 , and $\tilde{\tau}_1$, taking into account the mixing and the Yukawa couplings. In section 3 we give numerical results for the cross sections of $e^+e^- \rightarrow \tilde{t}_1 \tilde{t}_1^*, \tilde{b}_1 \tilde{b}_1^*, \tilde{\tau}_1 \tilde{\tau}_1^*$ for various masses as a function of the mixing angle, a numerical analysis of the decays of \tilde{t}_1 , \tilde{b}_1 , and $\tilde{\tau}_1$ into charginos and neutralinos, as well as a discussion of the main signatures. Section 4 contains a short summary and conclusions.

2 Production cross section and decay formulae

The mass matrix for stops, sbottoms and staus in the $(\tilde{f}_L, \tilde{f}_R)$ basis (with $\tilde{f} = \tilde{t}, \tilde{b}, \tilde{\tau}$) has the following form [6]:

$$\mathcal{M}_{\tilde{f}}^2 = \begin{pmatrix} m_{\tilde{f}_L}^2 & a_f m_f \\ a_f m_f & m_{\tilde{f}_R}^2 \end{pmatrix} \quad (1)$$

with

$$\begin{aligned} m_{\tilde{t}_L}^2 &= M_Q^2 + m_t^2 + m_Z^2 \cos 2\beta \left(\frac{1}{2} - \frac{2}{3} \sin^2 \theta_W\right), & m_{\tilde{t}_R}^2 &= M_U^2 + m_t^2 - \frac{2}{3} m_Z^2 \cos 2\beta \sin^2 \theta_W, \\ m_{\tilde{b}_L}^2 &= M_Q^2 + m_b^2 - m_Z^2 \cos 2\beta \left(\frac{1}{2} - \frac{1}{3} \sin^2 \theta_W\right), & m_{\tilde{b}_R}^2 &= M_D^2 + m_b^2 + \frac{1}{3} m_Z^2 \cos 2\beta \sin^2 \theta_W, \\ m_{\tilde{\tau}_L}^2 &= M_L^2 + m_\tau^2 - m_Z^2 \cos 2\beta \left(\frac{1}{2} - \sin^2 \theta_W\right), & m_{\tilde{\tau}_R}^2 &= M_E^2 + m_\tau^2 + m_Z^2 \cos 2\beta \sin^2 \theta_W, \end{aligned} \quad (2)$$

and

$$a_t m_t = m_t (A_t - \mu \cot \beta), \quad a_b m_b = m_b (A_b - \mu \tan \beta), \quad a_\tau m_\tau = m_\tau (A_\tau - \mu \tan \beta). \quad (3)$$

The mass eigenstates \tilde{f}_1 and \tilde{f}_2 are related to \tilde{f}_L and \tilde{f}_R by:

$$\begin{pmatrix} \tilde{f}_1 \\ \tilde{f}_2 \end{pmatrix} = \begin{pmatrix} \cos \theta_{\tilde{f}} & \sin \theta_{\tilde{f}} \\ -\sin \theta_{\tilde{f}} & \cos \theta_{\tilde{f}} \end{pmatrix} \begin{pmatrix} \tilde{f}_L \\ \tilde{f}_R \end{pmatrix} \quad (4)$$

with the eigenvalues

$$m_{\tilde{f}_{1,2}}^2 = \frac{1}{2}(m_{\tilde{f}_L}^2 + m_{\tilde{f}_R}^2) \mp \frac{1}{2}\sqrt{(m_{\tilde{f}_L}^2 - m_{\tilde{f}_R}^2)^2 + 4a_f^2 m_f^2}. \quad (5)$$

The mixing angle $\theta_{\tilde{f}}$ is given by

$$\cos \theta_{\tilde{f}} = -a_f m_f \sqrt{\frac{1}{(m_{\tilde{f}_L}^2 - m_{\tilde{f}_1}^2)^2 + a_f^2 m_f^2}}, \quad \sin \theta_{\tilde{f}} = \sqrt{\frac{(m_{\tilde{f}_L}^2 - m_{\tilde{f}_1}^2)^2}{(m_{\tilde{f}_L}^2 - m_{\tilde{f}_1}^2)^2 + a_f^2 m_f^2}}. \quad (6)$$

Hence, $|\cos \theta_{\tilde{f}}| > 1/\sqrt{2}$ if $m_{\tilde{f}_L} < m_{\tilde{f}_R}$ and $|\cos \theta_{\tilde{f}}| < 1/\sqrt{2}$ if $m_{\tilde{f}_R} < m_{\tilde{f}_L}$.

The reaction $e^+e^- \rightarrow \tilde{f}_1 \tilde{f}_1^*$ proceeds via γ and Z^0 exchange. The tree level cross section at a center-of-mass energy of \sqrt{s} is given by:

$$\sigma^{tree} = \frac{\pi\alpha^2 N_C}{3s} \beta^3 \left[Q_f^2 + \left(\frac{(v_e^2 + a_e^2) v_{\tilde{f}_1}^2}{16 s_W^4 c_W^4} s^2 - \frac{Q_f v_e v_{\tilde{f}_1}}{2 s_W^2 c_W^2} s(s - m_Z^2) \right) \frac{1}{(s - m_Z^2)^2 + \Gamma_Z^2 m_Z^2} \right] \quad (7)$$

where $s_W^2 = 1 - c_W^2 = \sin^2 \theta_W$, $v_e = 2 \sin^2 \theta_W - \frac{1}{2}$ and $a_e = -\frac{1}{2}$. N_C is a colour factor which is 3 for squarks and 1 for sleptons. The Z^0 coupling to $\tilde{f}_1 \tilde{f}_1^*$ is proportional $v_{\tilde{f}_1} = 2(I_f^3 \cos^2 \theta_{\tilde{f}} - Q_f \sin^2 \theta_W)$. Here I_f^3 and Q_f are the third component of the weak isospin and the charge of the fermion f ($Q_e = -1$). σ^{tree} shows the typical β^3 suppression where $\beta = (1 - 4m_{\tilde{f}_1}^2/s)^{1/2}$ is the velocity of the outgoing scalar particles. The interference of the γ and Z^0 exchange contributions leads to a characteristic minimum of the cross section at

$$\cos^2 \theta_{\tilde{f}}|_{min} = \frac{Q_f}{I_f^3} \sin^2 \theta_W \left[1 + \left(1 - \frac{s}{m_Z^2}\right) \cos^2 \theta_W \frac{L_e + R_e}{L_e^2 + R_e^2} \right] \quad (8)$$

where $L_e = \sin^2 \theta_W - \frac{1}{2}$ and $R_e = \sin^2 \theta_W$. The angular distribution has the familiar $\sin^2 \vartheta$ shape, with ϑ the scattering angle:

$$\frac{d\sigma^{tree}}{d\cos \vartheta} = \frac{3}{4} \sin^2 \vartheta \sigma^{tree}. \quad (9)$$

In the case of squarks QCD radiative corrections are important. The conventional QCD corrections were calculated in [7, 8] including the radiation of soft and hard gluons (in $\mathcal{O}(\alpha_s)$). The QCD corrections within the MSSM including virtual gluino and squark exchange were computed in [9] (The corrections due to the four-squark interaction is zero in the renormalization

scheme used). In our numerical calculations we have included both the gluonic corrections and those due to gluino and squark exchange. The corrections due to the exchange of supersymmetric particles are, however, small in the energy range of LEP2. Moreover, we have taken into account initial state radiation (ISR) [10].

The sfermion interaction with neutralinos and charginos is given by [11]:

$$\mathcal{L} = g \bar{f} (a_{ik}^f P_L + b_{ik}^f P_R) \tilde{\chi}_k^0 \tilde{f}_i + g \bar{f}' (l_{ij}^f P_L + k_{ij}^f P_R) \tilde{\chi}_j^+ \tilde{f}_i + \text{h.c.} \quad (10)$$

with

$$\begin{pmatrix} a_{1k}^f \\ a_{2k}^f \end{pmatrix} = \begin{pmatrix} \cos \theta_{\tilde{f}} & \sin \theta_{\tilde{f}} \\ -\sin \theta_{\tilde{f}} & \cos \theta_{\tilde{f}} \end{pmatrix} \begin{pmatrix} h_{Lk}^f \\ f_{Rk}^f \end{pmatrix}, \quad \begin{pmatrix} b_{1k}^f \\ b_{2k}^f \end{pmatrix} = \begin{pmatrix} \cos \theta_{\tilde{f}} & \sin \theta_{\tilde{f}} \\ -\sin \theta_{\tilde{f}} & \cos \theta_{\tilde{f}} \end{pmatrix} \begin{pmatrix} f_{Lk}^f \\ h_{Rk}^f \end{pmatrix}, \quad (11)$$

$$\begin{aligned} h_{Lk}^t &= Y_t (N_{k3} \sin \beta - N_{k4} \cos \beta), & f_{Lk}^t &= -\frac{2\sqrt{2}}{3} \sin \theta_W N_{k1} - \sqrt{2} \left(\frac{1}{2} - \frac{2}{3} \sin^2 \theta_W\right) \frac{N_{k2}}{\cos \theta_W}, \\ h_{Rk}^t &= Y_t (N_{k3} \sin \beta - N_{k4} \cos \beta), & f_{Rk}^t &= -\frac{2\sqrt{2}}{3} \sin \theta_W (\tan \theta_W N_{k2} - N_{k1}), \end{aligned} \quad (12)$$

$$\begin{aligned} h_{Lk}^b &= -Y_b (N_{k3} \cos \beta + N_{k4} \sin \beta), & f_{Lk}^b &= \frac{\sqrt{2}}{3} \sin \theta_W N_{k1} + \sqrt{2} \left(\frac{1}{2} - \frac{1}{3} \sin^2 \theta_W\right) \frac{N_{k2}}{\cos \theta_W}, \\ h_{Rk}^b &= -Y_b (N_{k3} \cos \beta + N_{k4} \sin \beta), & f_{Rk}^b &= \frac{\sqrt{2}}{3} \sin \theta_W (\tan \theta_W N_{k2} - N_{k1}), \end{aligned} \quad (13)$$

$$\begin{aligned} h_{Lk}^\tau &= -Y_\tau (N_{k3} \cos \beta + N_{k4} \sin \beta), & f_{Lk}^\tau &= \sqrt{2} \sin \theta_W N_{k1} + \sqrt{2} \left(\frac{1}{2} - \sin^2 \theta_W\right) \frac{N_{k2}}{\cos \theta_W}, \\ h_{Rk}^\tau &= -Y_\tau (N_{k3} \cos \beta + N_{k4} \sin \beta), & f_{Rk}^\tau &= \sqrt{2} \sin \theta_W (\tan \theta_W N_{k2} - N_{k1}), \end{aligned} \quad (14)$$

for the sfermion-fermion-neutralino interaction, and

$$\begin{aligned} l_{1j}^t &= -V_{j1} \cos \theta_{\tilde{t}} + Y_t V_{j2} \sin \theta_{\tilde{t}}, & k_{1j}^t &= Y_b U_{j2} \cos \theta_{\tilde{t}}, \\ l_{2j}^t &= V_{j1} \sin \theta_{\tilde{t}} + Y_t V_{j2} \cos \theta_{\tilde{t}}, & k_{2j}^t &= -Y_b U_{j2} \sin \theta_{\tilde{t}}, \end{aligned} \quad (15)$$

$$\begin{aligned} l_{1j}^b &= -U_{j1} \cos \theta_{\tilde{b}} + Y_b U_{j2} \sin \theta_{\tilde{b}}, & k_{1j}^b &= Y_t V_{j2} \cos \theta_{\tilde{b}}, \\ l_{2j}^b &= U_{j1} \sin \theta_{\tilde{b}} + Y_b U_{j2} \cos \theta_{\tilde{b}}, & k_{2j}^b &= -Y_t V_{j2} \sin \theta_{\tilde{b}}, \end{aligned} \quad (16)$$

$$\begin{aligned} l_{1j}^\tau &= -U_{j1} \cos \theta_{\tilde{\tau}} + Y_\tau U_{j2} \sin \theta_{\tilde{\tau}}, & k_{1j}^\tau &= 0, \\ l_{2j}^\tau &= U_{j1} \sin \theta_{\tilde{\tau}} + Y_\tau U_{j2} \cos \theta_{\tilde{\tau}}, & k_{2j}^\tau &= 0, \end{aligned} \quad (17)$$

for the sfermion-fermion-chargino interaction. N_{ij} is the 4×4 unitary matrix diagonalizing the neutral gaugino-higgsino mass matrix in the basis $\tilde{\gamma}, \tilde{Z}^0, \tilde{H}_1^0 \cos \beta - \tilde{H}_2^0 \sin \beta, \tilde{H}_1^0 \sin \beta + \tilde{H}_2^0 \cos \beta$ [12]. U_{ij} and V_{ij} are the 2×2 unitary matrices diagonalizing the charged gaugino-higgsino mass matrix [13]. We choose a phase convention in which N_{ij}, U_{ij} , and V_{ij} are real. Y_f denotes the Yukawa coupling,

$$Y_t = m_t / (\sqrt{2} m_W \sin \beta), \quad Y_b = m_b / (\sqrt{2} m_W \cos \beta), \quad Y_\tau = m_\tau / (\sqrt{2} m_W \cos \beta). \quad (18)$$

The respective decay widths then are

$$\Gamma(\tilde{f}_i \rightarrow f \tilde{\chi}_k^0) = \frac{g^2 \lambda^{\frac{1}{2}}(m_{\tilde{f}_i}^2, m_f^2, m_{\tilde{\chi}_k^0}^2)}{16\pi m_{\tilde{f}_i}^3} \left[(a_{ik}^2 + b_{ik}^2)(m_{\tilde{f}_i}^2 - m_f^2 - m_{\tilde{\chi}_k^0}^2) - 4a_{ik}b_{ik}m_fm_{\tilde{\chi}_k^0} \right] \quad (19)$$

and

$$\Gamma(\tilde{f}_i \rightarrow f' \tilde{\chi}_j^\pm) = \frac{g^2 \lambda^{\frac{1}{2}}(m_{\tilde{f}_i}^2, m_{f'}^2, m_{\tilde{\chi}_j^\pm}^2)}{16\pi m_{\tilde{f}_i}^3} \left[(l_{ij}^2 + k_{ij}^2)(m_{\tilde{f}_i}^2 - m_{f'}^2 - m_{\tilde{\chi}_j^\pm}^2) - 4l_{ij}k_{ij}m_{f'}m_{\tilde{\chi}_j^\pm} \right] \quad (20)$$

where $\lambda(x, y, z) = x^2 + y^2 + z^2 - 2xy - 2xz - 2yz$.

3 Numerical results

3.1 Stop \tilde{t}_1

The total cross sections for the process $e^+e^- \rightarrow \tilde{t}_1 \bar{\tilde{t}}_1$ at $\sqrt{s} = 175$ GeV and $\sqrt{s} = 192.5$ GeV are shown in Fig. 1 as a function of $|\cos \theta_{\tilde{t}}|$ for several mass values of \tilde{t}_1 . At $\sqrt{s} = 192.5$ (175) GeV, for a stop mass of 80 GeV the cross section reaches 0.35 (0.18) pb. Assuming an integrated luminosity of 300 (500) pb^{-1} at $\sqrt{s} = 192.5$ (175) GeV one can thus expect ~ 60 to 105 (50 to 90) $\tilde{t}_1 \bar{\tilde{t}}_1$ events for $m_{\tilde{t}_1} \simeq 80$ GeV. Moreover, the cross section shows a clear dependence on the mixing angle for $m_{\tilde{t}_1} \lesssim 80$ GeV and $|\cos \theta_{\tilde{t}}| \gtrsim 0.6$. In this region cross section measurements should therefore allow to determine the stop mixing angle once the mass of \tilde{t}_1 is known. The importance of radiative corrections is illustrated in Fig. 2, where we show the conventional QCD corrections in $\mathcal{O}(\alpha_s)$, the corrections due to gluino exchange as well as the ISR corrections at $\sqrt{s} = 192.5$ GeV as a function of $m_{\tilde{t}_1}$ for $\cos \theta_{\tilde{t}} = 0.7$. The gluonic corrections enhance the tree level cross section rising from 17 to 41% for stop masses in the range of 45 to 85 GeV. The corrections due to the exchange of supersymmetric particles are $\lesssim 1.2\%$ for $m_{\tilde{g}} = 200$ GeV and $m_{\tilde{t}_2} = 250$ GeV and depend on the stop mixing angle. Initial state radiation turns out to alter the tree level cross section from $\sim 1.2\%$ to $\sim -21\%$ for $m_{\tilde{t}_1} = 45$ to 85 GeV.

Assuming $m_{\tilde{t}_1} < m_{\tilde{t}_2}$ the main decay modes of \tilde{t}_1 are $\tilde{t}_1 \rightarrow c \tilde{\chi}_1^0$ and $\tilde{t}_1 \rightarrow b \tilde{\chi}_1^+$. The latter decay has practically 100% branching ratio if it is kinematically allowed. As $\tilde{\chi}_1^+$ further decays

into $\tilde{\chi}_1^0 q\bar{q}'$ or $\tilde{\chi}_1^0 \ell\bar{\nu}_\ell$ the signature is two acoplanar b jets accompanied by two leptons + large missing energy (\cancel{E}), or single lepton + jets + \cancel{E} , or jets + \cancel{E} . Here the b tagging technique can be used to extract the signal. Moreover, in this case the $\tilde{\chi}_1^+$ will most likely be observed first and the information from its decay properties can then be used to identify the \tilde{t}_1 . On the other hand, if $m_{\tilde{t}_1} < m_{\tilde{\chi}_1^+} + m_b$ the flavour changing decay $\tilde{t}_1 \rightarrow c \tilde{\chi}_1^0$ has practically 100% branching ratio. The signature is then two acoplanar jets + \cancel{E} . Generally, for $\tilde{t}_1 \rightarrow c \tilde{\chi}_1^0$ the invisible energy is larger than in case of $\tilde{t}_1 \rightarrow b \tilde{\chi}_1^+$. In Fig. 3 we show the domains of the \tilde{t}_1 decay modes in the (M, μ) plane for $m_{\tilde{t}_1} = 80$ GeV and $\tan\beta = 2$ (there is a small stripe where the decay $\tilde{t}_1 \rightarrow c \tilde{\chi}_2^0$ is also possible). If, however, $m_{\tilde{\chi}_1^\pm} + m_b > m_{\tilde{t}_1} > m_{\tilde{\ell}(\tilde{\nu})} + m_b (+m_\ell)$ the decays $\tilde{t}_1 \rightarrow b \nu_\ell \tilde{\ell}$ or $\tilde{t}_1 \rightarrow b \bar{\ell} \tilde{\nu}_\ell$, proceeding via a virtual $\tilde{\chi}_1^+$ can compete with the decay into $c \tilde{\chi}_1^0$. In this case the signature is again $2b + 2\ell + \cancel{E}$.

If the lifetime of \tilde{t}_1 is longer than the typical hadronization time of $\mathcal{O}(10^{-23} \text{ s})$, i. e. $\Gamma \lesssim 0.2$ GeV, \tilde{t}_1 hadronizes first into a colourless $(\tilde{t}_1\bar{q})$ or (\tilde{t}_1qq) bound state before decaying. This is generally expected in case of $\tilde{t}_1 \rightarrow c \tilde{\chi}_1^0$ and $\tilde{t}_1 \rightarrow b \nu_\ell \tilde{\ell}$, $b \bar{\ell} \tilde{\nu}_\ell$ since these decays involve the electroweak coupling twice [14]. However, also the width of the \tilde{t}_1 decay into $b \tilde{\chi}_1^+$ can be smaller than the hadronization scale as illustrated in Fig. 4. Here we show the width of $\tilde{t}_1 \rightarrow b \tilde{\chi}_1^+$ as a function of $\cos\theta_{\tilde{t}}$ for $m_{\tilde{t}_1} = 85$ GeV, $m_{\tilde{\chi}_1^\pm} \simeq 60$ GeV, $\tan\beta = 2$, and three scenarios with $M \ll |\mu|$, $|\mu| \ll M$, and $M \sim |\mu|$ respectively.

If, as for the curves (a) and (b), M is much smaller than $|\mu|$ the lighter chargino is gaugino-like. In this case the \tilde{t}_1 - b - $\tilde{\chi}_1^-$ interaction is dominated by $V_{11} \cos\theta_{\tilde{t}}$ in eq. (15) for $|\cos\theta_{\tilde{t}}| \gtrsim 0.3$. The deviation of the decay width from the $\cos^2\theta_{\tilde{t}}$ shape and the asymmetry in the sign of μ are due to constructive and destructive interferences with the term proportional to the top Yukawa coupling ($Y_t V_{12} \sin\theta_{\tilde{t}}$) which becomes especially important for $\tilde{t}_1 \sim \tilde{t}_R$ and increases with decreasing $|\mu|$.

On the other hand, a higgsino-like $\tilde{\chi}_1^+$ strongly couples to \tilde{t}_R , the dominant coupling being proportional to the top Yukawa coupling ($|\mu| \ll M$, curves (c) and (d)). Thus the decay width is large if $|\cos\theta_{\tilde{t}}| \sim 0$ but goes to zero for $\tilde{t}_1 \sim \tilde{t}_L$.

For $M \sim |\mu|$, which is shown in (e) and (f), a complicated interplay of gaugino and higgsino couplings gives rise to an intricate dependence on the mixing angle and a large asymmetry in

the sign of μ .

The process of fragmentation of \tilde{t}_1 was discussed in detail in ref. [8]. Fast moving stops first radiate off gluons at small angles. This process can be treated perturbatively. After that the (non-perturbative) hadronization phase follows by forming $(\tilde{t}_1\bar{q})$ and (\tilde{t}_1qq) hadrons. For $\beta \sim 1/2$ the energy loss of \tilde{t}_1 due to gluon radiation and due to hadronization is of comparable size. Near the threshold, the gluon emission suffers a β^4 suppression.

Monte Carlo studies for \tilde{t}_1 pair production have been performed within the CERN-LEP2 Workshop 1995 [15]. They have mainly concentrated on the decay $\tilde{t}_1 \rightarrow c\tilde{\chi}_1^0$ since in this case \tilde{t}_1 would most probably be the first SUSY particle to be discovered. For the simulation of \tilde{t}_1 fragmentation different approaches have been used. The conclusions have been a 5σ discovery reach of $m_{\tilde{t}_1} \simeq 75$ to 90 GeV and a 95% CL exclusion of $m_{\tilde{t}_1} \simeq 84$ to 92 GeV at $\sqrt{s} = 190$ GeV, for $\mathcal{L} = 300 \text{ pb}^{-1}$ depending on the stop mixing angle and the mass of the lightest neutralino. In case of $\tilde{t}_1 \rightarrow b\tilde{\chi}_1^+$ the experimental reach for $m_{\tilde{t}_1}$ is ~ 85 GeV.

3.2 Sbottom \tilde{b}_1

According to eq. (3) a considerable \tilde{b}_L - \tilde{b}_R mixing is possible if $\tan\beta$ is large ($\tan\beta > 10$). In this case the sbottom \tilde{b}_1 can be rather light. Hence, it is also interesting to discuss \tilde{b}_1 search at LEP2.

The total (SUSY-QCD & ISR corrected) cross sections of \tilde{b}_1 pair production at $\sqrt{s} = 175$ GeV and $\sqrt{s} = 192.5$ GeV are shown in Fig. 5 as a function of $|\cos\theta_{\tilde{b}}|$ for several mass values of \tilde{b}_1 . As can be seen, the dependence on the mixing angle is even more pronounced than in case of \tilde{t}_1 production. The cross section of $e^+e^- \rightarrow \tilde{b}_1\tilde{b}_1$ is smaller than the $\tilde{t}_1\tilde{t}_1$ cross section by a factor of 4 to $\sim 5/4$ for $|\cos\theta_{\tilde{b}}|$ in the range of 0 to 1. Again, radiative corrections are important. Standard QCD and ISR corrections are similar to the stop case, i. e. gluon corrections enhancing the tree level cross section from 17 to 41% for \tilde{b}_1 masses in the range of 45 to 85 GeV and initial state radiation lowering it by up to 21%. The corrections due to gluino exchange are $\lesssim 1\%$ for $m_{\tilde{g}} = 200$ GeV and $m_{\tilde{b}_2} = 250$ GeV.

Assuming $m_{\tilde{b}_1} < m_{\tilde{g}}$ the main decay modes of \tilde{b}_1 are $\tilde{b}_1 \rightarrow b \tilde{\chi}_1^0$ and $\tilde{b}_1 \rightarrow b \tilde{\chi}_2^0$, the second decay being possible in the parameter region approximately given by $M < m_{\tilde{b}_1} - m_b$ or $|\mu| < m_{\tilde{b}_1} - m_b$. For the $b \tilde{\chi}_1^0$ channel the signature is two acoplanar b jets + missing energy \cancel{E} . If the \tilde{b}_1 decays into $b \tilde{\chi}_2^0$ the b jets are accompanied by additional jets and/or leptons from $\tilde{\chi}_2^0 \rightarrow \tilde{\chi}_1^0 q \bar{q}$ and/or $\tilde{\chi}_2^0 \rightarrow \tilde{\chi}_1^0 \ell \bar{\ell}$. b tagging will help to enhance the signal. The domains of the \tilde{b}_1 decays in the (M, μ) plane are shown in Fig. 6 for $m_{\tilde{b}_1} = 80$ GeV and $\tan \beta = 40$.

In Fig. 7 we show the branching ratio for $\tilde{b}_1 \rightarrow b \tilde{\chi}_1^0$ as a function of $\cos \theta_{\tilde{b}}$ for $m_{\tilde{b}_1} = 80$ GeV, $\tan \beta = 40$, $|\mu| = 500$ GeV, and $M = 55, 65,$ and 75 GeV. As can be seen, the branching ratio is highly dependent on the mixing angle, if $M \ll |\mu|$ and both $\tilde{\chi}_1^0$ and $\tilde{\chi}_2^0$ are light. In this case \tilde{b}_1 mainly decays into $b \tilde{\chi}_1^0$ if $|\cos \theta_{\tilde{b}}| \sim 0$, whereas for $\tilde{b}_1 \sim \tilde{b}_L$ the decay into $b \tilde{\chi}_2^0$ dominates. Evidently, the dependence on the mixing angle weakens with increasing $\tilde{\chi}_2^0$ masses. If, however, $M \sim |\mu|$ or $M \gg |\mu|$ the decay $\tilde{b}_1 \rightarrow b \tilde{\chi}_1^0$ is the dominant mode. The μ dependence of the branching ratio is shown in Fig. 8 for $m_{\tilde{b}_1} = 80$ GeV, $|\cos \theta_{\tilde{b}}| = 0.72$, $\tan \beta = 40$, and several values of M . As the parameter A_b should not become unnaturally large in supergravity models [16], for large values of $\tan \beta$, the parameter μ determines the sign of $\cos \theta_{\tilde{b}}$ (see eq. (3) and eq. (6)). For this reason, we have chosen $\cos \theta_{\tilde{b}}$ and μ such that they have the same sign in Fig. 7, Fig. 8, and Fig. 9.

As in the \tilde{t}_1 case the decay width of \tilde{b}_1 can be significantly smaller than 0.2 GeV as illustrated in Fig. 9. Here we show the total width of \tilde{b}_1 as a function of μ for $m_{\tilde{b}_1} = 80$ GeV, $|\cos \theta_{\tilde{b}}| = 0.72$, $\tan \beta = 40$, and several values of M . The decay width only exceeds the hadronization scale ($\Gamma \gtrsim 0.2$ GeV) if $\tilde{\chi}_1^0$ is very light ($\lesssim 30$ GeV) or if the light neutralinos have strong higgsino components (small $|\mu|$). It clearly increases with decreasing $|\mu|$ as then $\tilde{\chi}_{1,2}^0$ become lighter and the higgsino couplings proportional to Y_b gain importance. So does the dependence on the mixing angle, which shows minima at $\cos \theta_{\tilde{b}} = \pm 1$ and $\cos \theta_{\tilde{b}} = 0$ where one decay channel ($b \tilde{\chi}_1^0$ or $b \tilde{\chi}_2^0$) dominates.

DELPHI has studied \tilde{b}_1 search when \tilde{b}_1 decays into $b \tilde{\chi}_1^0$ [15]. Their conclusion was that in this case the discovery potential for \tilde{b}_1 is similar to the one of $\tilde{t}_1 \rightarrow c \tilde{\chi}_1^0$, i. e. $m_{\tilde{b}_1} \lesssim 75$ to 90 GeV depending on $\theta_{\tilde{b}}$ and $m_{\tilde{\chi}_1^0}$.

3.3 Stau $\tilde{\tau}_1$

As in the sbottom sector one expects large $\tilde{\tau}_L$ - $\tilde{\tau}_R$ mixing for high values of $\tan\beta$. This would lead to a light $\tilde{\tau}_1$ which could also lie in the energy range of LEP2.

The $\tilde{\tau}_1 \bar{\tilde{\tau}}_1$ production cross sections are plotted in Fig. 10 at $\sqrt{s} = 175$ GeV and $\sqrt{s} = 192.5$ GeV as a function of $|\cos\theta_{\tilde{\tau}}|$ for several $\tilde{\tau}_1$ masses. As can be seen, the dependence on the mixing angle is much weaker for $\tilde{\tau}_1 \bar{\tilde{\tau}}_1$ than for $\tilde{t}_1 \bar{\tilde{t}}_1$ and $\tilde{b}_1 \bar{\tilde{b}}_1$ production. At $\sqrt{s} = 192.5$ GeV the cross section is of $\mathcal{O}(0.1)$ pb for $m_{\tilde{\tau}_1} = 80$ GeV and goes up to 0.55 pb for a $\tilde{\tau}_1$ mass of 50 GeV. This corresponds to a production rate of ~ 30 (25) events at $\sqrt{s} = 192.5$ (175) GeV for an integrated luminosity of $\mathcal{L} = 300$ (500) pb^{-1} and $m_{\tilde{\tau}_1} = 80$ GeV. Of course, here only ISR corrections have to be taken into account.

The simplest signature of $\tilde{\tau}_1 \bar{\tilde{\tau}}_1$ production is $2\tau + \cancel{E}$ with the τ leptons coming from $\tilde{\tau}_1 \rightarrow \tau \tilde{\chi}_1^0$ decays. If the decay modes into $\tau \tilde{\chi}_2^0$ and $\tilde{\nu}_\tau \tilde{\chi}_1^-$ are also kinematically accessible the signature is $2\tau + \text{jets and/or leptons} + \cancel{E}$, or single $\tau + \text{jets and/or leptons} + \cancel{E}$, or jets and/or leptons + \cancel{E} due to cascade decays of $\tilde{\chi}_2^0$ and $\tilde{\chi}_1^-$. The latter case occurs when both staus decay via $\tilde{\tau}_1 \rightarrow \tilde{\nu}_\tau \tilde{\chi}_1^-$ ($\bar{\tilde{\tau}}_1 \rightarrow \bar{\tilde{\nu}}_\tau \tilde{\chi}_1^+$). The parameter domains of the various $\tilde{\tau}_1$ decays in the (M, μ) plane are shown in Fig. 11 for $m_{\tilde{\tau}_1} = 80$ GeV and $\tan\beta = 40$. If \tilde{e} , $\tilde{\mu}$, and/or $\tilde{\nu}$ are lighter than $\tilde{\tau}_1$ then also three-body decays into these particles plus neutrino(s), lepton(s), or quark pairs are possible.

In Fig. 12 we show the branching ratios of $\tilde{\tau}_1$ decays into $\tau \tilde{\chi}_1^0$, $\tau \tilde{\chi}_2^0$, and $\nu_\tau \tilde{\chi}_1^-$ as a function of $\cos\theta_{\tilde{\tau}}$ for $m_{\tilde{\tau}_1} = 80$ GeV, $\tan\beta = 40$, (a) $M \ll |\mu|$, and (b) $|\mu| \ll M$. As in section 3.2, we have chosen $\cos\theta_{\tilde{\tau}}$ and μ such that they have the same sign in order to avoid unnaturally large values of A_τ . In case (a), i. e. $M \ll |\mu|$, if $\cos\theta_{\tilde{\tau}} \lesssim 0.5$ the decay $\tilde{\tau}_1 \rightarrow \tau \tilde{\chi}_1^0$ has $\gtrsim 80\%$ branching ratio as $\tilde{\tau}_R$ does not couple to a gaugino-like $\tilde{\chi}_2^0$ or $\tilde{\chi}_1^-$. On the other hand, the decays into $\tau \tilde{\chi}_2^0$ and $\tilde{\nu}_\tau \tilde{\chi}_1^-$ play an important rôle for $\tilde{\tau}_1 \sim \tilde{\tau}_L$, i. e. $\cos\theta_{\tilde{\tau}} \sim 1$. In contrast to that, for higgsino-like light neutralinos and charginos, i. e. $|\mu| \ll M$ as shown in (b), $\text{BR}(\tilde{\tau}_1 \rightarrow \tau \tilde{\chi}_1^0)$ and $\text{BR}(\tilde{\tau}_1 \rightarrow \tilde{\nu}_\tau \tilde{\chi}_1^-)$ are of comparable size for $\tilde{\tau}_1 \sim \tilde{\tau}_R$, whereas for $\tilde{\tau}_1 \sim \tilde{\tau}_L$ the $\tilde{\tau}_1$ - ν_τ - $\tilde{\chi}_1^-$ coupling vanishes and the decay into $\tau \tilde{\chi}_1^0$ has $\sim 100\%$ branching ratio. The $\tilde{\tau}_1 \rightarrow \tau \tilde{\chi}_2^0$ decay mode is negligible in this case.

For staus a new interesting aspect comes into play: Due to the supersymmetric versions of gauge and Yukawa interactions the sfermion-fermion-gaugino interaction conserves chirality while the sfermion-fermion-higgsino interaction flips it. The polarization of the final state fermion thus depends on the sfermion (L-R) mixing as well as on the gaugino-higgsino mixing. As, in contrast to other leptons, taus decay in the detector, one can determine their average polarization through the energy distribution of their decay products [17]. Hence, one has an additional opportunity to obtain information on the $\tilde{\tau}_L$ - $\tilde{\tau}_R$ and the gaugino-higgsino mixing by measuring the average polarization of tau leptons coming from $\tilde{\tau}_1 \rightarrow \tau \tilde{\chi}_k^0$ decays [18].

The average polarization of the τ leptons is given by:

$$\bar{\mathcal{P}}(\tau) = \frac{\sum_k \text{BR}(\tilde{\tau}_1 \rightarrow \tau_R \tilde{\chi}_k^0) - \text{BR}(\tilde{\tau}_1 \rightarrow \tau_L \tilde{\chi}_k^0)}{\sum_k \text{BR}(\tilde{\tau}_1 \rightarrow \tau_R \tilde{\chi}_k^0) + \text{BR}(\tilde{\tau}_1 \rightarrow \tau_L \tilde{\chi}_k^0)} \quad (21)$$

$\bar{\mathcal{P}}(\tau)$ depends on the stau mixing angle $\theta_{\tilde{\tau}}$ and on the mixing matrix N_{ij} of the neutral gaugino-higgsino sector. If the lighter neutralinos are gaugino-like only N_{k1} and N_{k2} give sizeable contributions. Thus, in this case $\bar{\mathcal{P}}(\tau) \simeq +1$ for $|\cos \theta_{\tilde{\tau}}| \simeq 0$, whereas $\bar{\mathcal{P}}(\tau) \simeq -1$ for $|\cos \theta_{\tilde{\tau}}| \simeq 1$. On the other hand, in case of higgsino-like $\tilde{\chi}_1^0$ and $\tilde{\chi}_2^0$, one finds $\bar{\mathcal{P}}(\tau) \simeq -1$ for $|\cos \theta_{\tilde{\tau}}| \simeq 0$ and $\bar{\mathcal{P}}(\tau) \simeq +1$ for $|\cos \theta_{\tilde{\tau}}| \simeq 1$. This is illustrated in Fig. 12 where we show the average polarization of tau leptons arising from $\tilde{\tau}_1 \rightarrow \tau \tilde{\chi}_k^0$ decays as a function of $\cos \theta_{\tilde{\tau}}$ for $m_{\tilde{\tau}_1} = 80$ GeV, $\tan \beta = 40$, and three scenarios of (a) $M \ll |\mu|$, (b) $|\mu| \ll M$, and (c) $M \sim |\mu|$. In case of $M \sim |\mu|$ where the lighter neutralinos have both, gaugino and higgsino, properties $\bar{\mathcal{P}}(\tau) \sim \frac{1}{2}$ and varies only little with the stau mixing angle.

OPAL has studied the experimental aspects of a stau search at LEP2 for $m_{\tilde{\tau}_R} \ll m_{\tilde{\tau}_L}$ [15]. At $\sqrt{s} = 190$ GeV and for $\mathcal{L} = 300 \text{ pb}^{-1}$ they obtained a 5σ detectability for stau pairs of $m_{\tilde{\tau}_R} \simeq 70$ to 83 GeV for neutralino masses in the range of 20 to 72 GeV. However, they have neglected the interesting possibility of $\tilde{\tau}_L$ - $\tilde{\tau}_R$ mixing.

4 Conclusions

We have discussed the phenomenology of stop, sbottom, and stau pair production and decays at LEP2 paying particular attention to the sfermion L-R mixing. Analytical formulae have

been given for the sfermion mixing, for the cross sections of \tilde{t}_1 , \tilde{b}_1 , and $\tilde{\tau}_1$ pair production in e^+e^- annihilation, and for the widths of the decays of these particles into neutralinos and charginos. We have presented numerical predictions for these production and decay processes and analyzed their dependence on the SUSY parameters. It has turned out that due to L-R mixing and non-negligible Yukawa couplings the phenomenology of stops, sbottoms, and staus can be significantly different from that of first and second generation sfermions. Moreover, we have shown that in case of \tilde{t}_1 and \tilde{b}_1 hadronization effects can be important. For $\tilde{\tau}_1$ we have also discussed the dependence of the average polarization of taus arising from $\tilde{\tau}_1 \rightarrow \tau \tilde{\chi}_k^0$ decays on $\tilde{\tau}_L$ - $\tilde{\tau}_R$ and gaugino-higgsino mixing.

Acknowledgements

We thank our colleagues from the “New Particles” working group of the 1995 CERN–LEP2 workshop for useful discussions. This work was supported by the ”Fonds zur Förderung der wissenschaftlichen Forschung” of Austria, project no. P10843-PHY.

References

- [1] For a review, see
H. P. Nilles, Phys. Rep. 110 (1984) 1
H.E. Haber, G.L. Kane, Phys. Rep. 117 (1985) 75
R. Barbieri, Riv. Nuov. Cim. 11 (1988) 1
- [2] Review of Particle Properties, Particle Data Group, Phys. Rev. D50 (1994) 1173
- [3] J.-F. Grivaz, Rapporteur Talk, International Europhysics Conference on High Energy Physics, Brussels, 1995
- [4] L. Rolandi (ALEPH), H. Dijkstra (DELPHI), D. Strickland (L3), G. Wilson (OPAL), Joint Seminar on the First Results of LEP1.5, CERN, December 12, 1995
ALEPH Coll., CERN–PPE/96-10, Jan. 1996
L3 Coll., H. Nowak and A. Sopczak, L3 Note 1887, Jan. 1996
OPAL Coll., S. Asai and S. Komamiya, OPAL Physics Note PN-205, Feb. 1996
- [5] The D \emptyset collaboration, FERMILAB-Conf-95/186-E, proc. of the *10th Topical Workshop on Proton-Antiproton Collider Physics*, FNAL (1995)

- [6] J. Ellis, S. Rudaz, Phys. Lett. B128 (1983) 248
J.F. Gunion, H.E. Haber, Nucl. Phys. B272 (1986) 1
- [7] M. Drees, K. Hikasa, Phys. Lett. B252 (1990) 127
- [8] W. Beenakker, R. Höpker, P. M. Zerwas, Phys. Lett. B349 (1995) 463
- [9] H. Eberl, A. Bartl, W. Majerotto, UWThPh-1996-6, HEPHY-PUB 640/96
- [10] See, e.g. M. Peskin, 17th SLAC Summer Institute, *Physics at the 100 GeV mass scale*, SLAC-PUB-5210 (1990)
- [11] A. Bartl, W. Majerotto, W. Porod, Z. Phys. C 64 (1994) 499
A. Bartl, W. Majerotto, B. Mösslacher, N. Oshimo, S. Stippel, Phys. Rev. D43 (1991) 2214
- [12] A. Bartl, H. Fraas, W. Majerotto, Nucl. Phys. B278 (1986) 1
- [13] A. Bartl, H. Fraas, W. Majerotto, B. Mösslacher, Z. Phys. C 55 (1992) 257
- [14] K. Hikasa, M. Kobayashi, Phys. Rev. D36 (1987) 724
- [15] *Searches for new physics* section in Vol. I of the Proc. of the *The Workshop on Physics at LEP2* (G. Altarelli, T. Sjöstrand, F. Zwirner, eds.), CERN 1995
- [16] For a review, see e.g., M. Drees and S.P. Martin, Wisconsin preprint, MADPH-95-879
- [17] Y. S. Tsai, Phys. Rev. D4 (1971) 2821
T. Hagiwara, S. Y. Pi, A. I. Sanda, Ann. of Physics 106 (1977) 134
H. Kühn, F. Wagner, Nucl. Phys. B236 (1984) 16
M. Chen, C. Dionisi, M. Martinez, X. Tata, Phys. Rep. (1988) 201
C. Dionisi et al., Proc. of the ECFA Workshop on LEP200. Aachen, 1986, Vol. II, p. 380, CERN 87-08, ECFA 87/108
- [18] M. M. Nojiri, Phys. Rev. D51 (1995) 6281

Figure captions

Figure 1: Total cross section for $e^+e^- \rightarrow \tilde{t}_1 \tilde{t}_1^*$ in pb at $\sqrt{s} = 175$ GeV (dashed lines) and $\sqrt{s} = 192.5$ GeV (solid lines) as a function of the stop mixing angle for \tilde{t}_1 masses of 50, 60, 70, 80, and 90 GeV.

Figure 2: Gluon, gluino-stop, initial state, and total radiative corrections relative to the tree level cross section of $e^+e^- \rightarrow \tilde{t}_1 \tilde{t}_1^*$ at $\sqrt{s} = 192.5$ GeV as a function of $m_{\tilde{t}_1}$ for $\cos \theta_{\tilde{t}} = 0.7$.

Figure 3: Parameter domains in the (M, μ) plane for the various \tilde{t}_1 decay modes, for $m_{\tilde{t}_1} = 80$ GeV and $\tan \beta = 2$. The grey area is excluded by LEP1.

Figure 4: Decay width of $\tilde{t}_1 \rightarrow b \tilde{\chi}_1^+$ for $m_{\tilde{t}_1} = 85$ GeV, $m_{\tilde{\chi}_1^-} \simeq 60$ GeV, $\tan \beta = 2$, (a) $M = 51.2$ GeV, $\mu = -500$ GeV, (b) $M = 72.0$ GeV, $\mu = +500$ GeV, (c) $M = 400$ GeV, $\mu = -49.4$ GeV, (d) $M = 400$ GeV, $\mu = +75.5$ GeV, (e) $M = 50$ GeV, $\mu = -47.9$ GeV, and (f) $M = 135$ GeV, $\mu = +132$ GeV.

Figure 5: Total cross section for $e^+e^- \rightarrow \tilde{b}_1 \tilde{b}_1^*$ in pb at $\sqrt{s} = 175$ GeV (dashed lines) and $\sqrt{s} = 192.5$ GeV (solid lines) as a function of the sbottom mixing angle for \tilde{b}_1 masses of 50, 60, 70, 80, and 90 GeV.

Figure 6: Parameter domains in the (M, μ) plane for the \tilde{b}_1 decay modes for $m_{\tilde{b}_1} = 80$ GeV and $\tan \beta = 40$, (a) $\tilde{b}_1 \rightarrow b \tilde{\chi}_1^0$ and (b) $\tilde{b}_1 \rightarrow b \tilde{\chi}_{1,2}^0$. The grey area is excluded by LEP1.

Figure 7: Branching ratio of $\tilde{b}_1 \rightarrow b \tilde{\chi}_1^0$ in percent as a function of the sbottom mixing angle for $m_{\tilde{b}_1} = 80$ GeV, $\tan \beta = 40$, $|\mu| = 500$ GeV, and $M = 55, 65, \text{ and } 75$ GeV.

Figure 8: Branching ratio of $\tilde{b}_1 \rightarrow b \tilde{\chi}_1^0$ in percent as a function of μ for $m_{\tilde{b}_1} = 80$ GeV, $\cos \theta_{\tilde{b}} = 0.72$, $\tan \beta = 40$, and $M = 55, 65, \text{ and } 75$ GeV.

Figure 9: Total decay width of \tilde{b}_1 in GeV as a function of μ for $m_{\tilde{b}_1} = 80$ GeV, $\cos \theta_{\tilde{b}} = 0.72$, $\tan \beta = 40$, and $M = 55, 65, 75, \text{ and } 150$ GeV.

Figure 10: Total cross section for $e^+e^- \rightarrow \tilde{\tau}_1 \tilde{\tau}_1^*$ in pb at $\sqrt{s} = 175$ GeV (dashed lines) and $\sqrt{s} = 192.5$ GeV (solid lines) as a function of the stau mixing angle for $\tilde{\tau}_1$ masses of 50, 60, 70, 80, and 90 GeV.

Figure 11: Parameter domains in the (M, μ) plane for the various $\tilde{\tau}_1$ decay modes, for $m_{\tilde{\tau}_1} = 80$ GeV and $\tan\beta = 40$ with (a) $\tilde{\tau}_1 \rightarrow \tau \tilde{\chi}_1^0$, (b) $\tilde{\tau}_1 \rightarrow \tau \tilde{\chi}_1^0, \nu_\tau \tilde{\chi}_1^-$, and (c) $\tilde{\tau}_1 \rightarrow \tau \tilde{\chi}_1^0, \tau \tilde{\chi}_2^0, \nu_\tau \tilde{\chi}_1^-$. The grey area is excluded by LEP1.

Figure 12: Branching ratio of $\tilde{\tau}_1 \rightarrow \tau \tilde{\chi}_1^0$ (solid lines), $\tilde{\tau}_1 \rightarrow \tau \tilde{\chi}_2^0$ (dashed lines), and $\tilde{\tau}_1 \rightarrow \nu_\tau \tilde{\chi}_1^-$ (dashdotted lines) in percent as a function of the stau mixing angle for $m_{\tilde{\tau}_1} = 80$ GeV, $\tan\beta = 40$, (a) $M = 65$ GeV, $|\mu| = 500$ GeV, and (b) $M = 300$ GeV, $|\mu| = 60$ GeV.

Figure 13: Average polarization of τ leptons arising from $\tilde{\tau}_1 \rightarrow \tau \tilde{\chi}_k^0$ decays as a function of the stau mixing angle for $m_{\tilde{\tau}_1} = 80$ GeV, $\tan\beta = 40$, (a) $M = 65$ GeV, $|\mu| = 500$ GeV (solid line), (b) $M = 300$ GeV, $|\mu| = 60$ GeV (dashdotted line), and (c) $M = 100$ GeV, $|\mu| = 100$ GeV (dashed line).

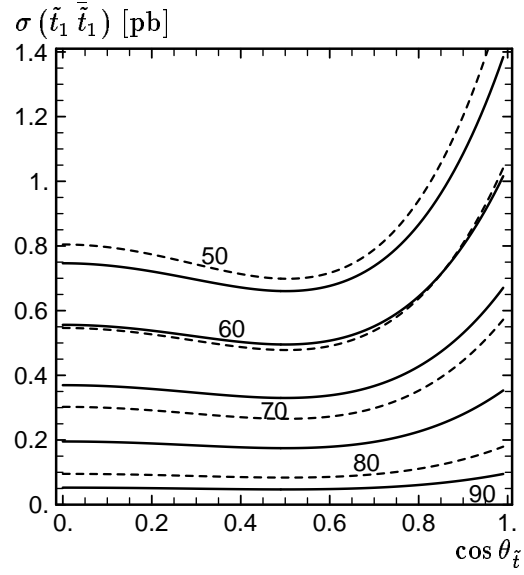


Figure 1

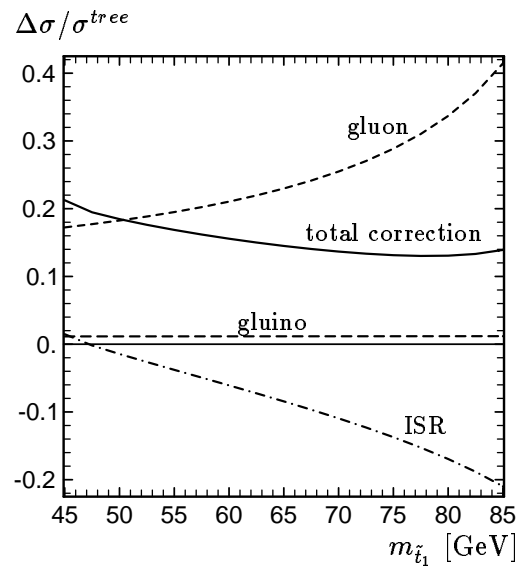


Figure 2

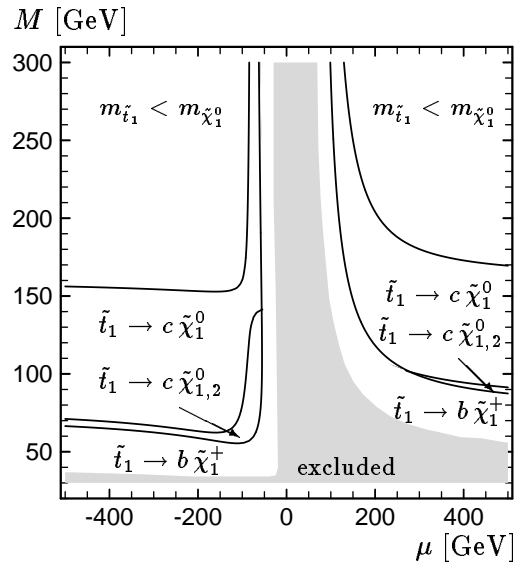


Figure 3

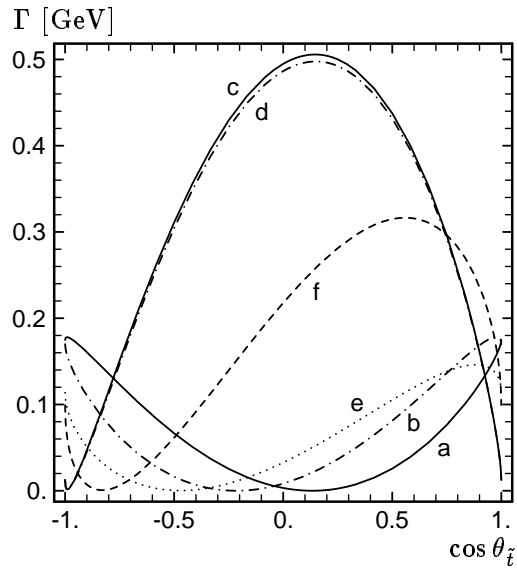


Figure 4

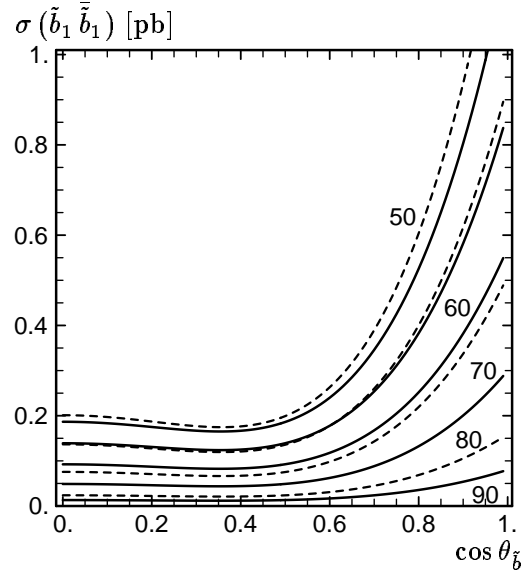


Figure 5

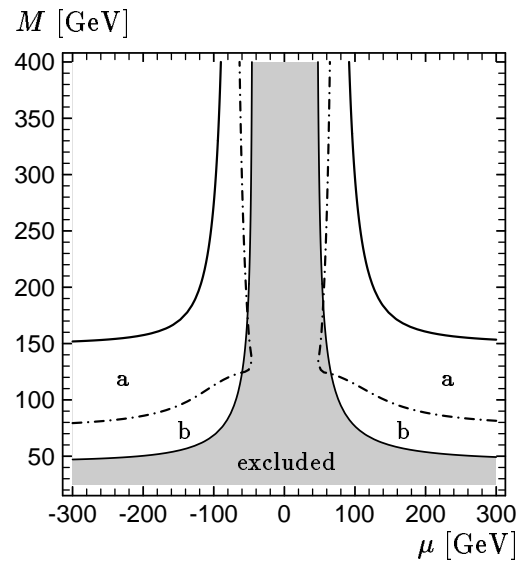


Figure 6

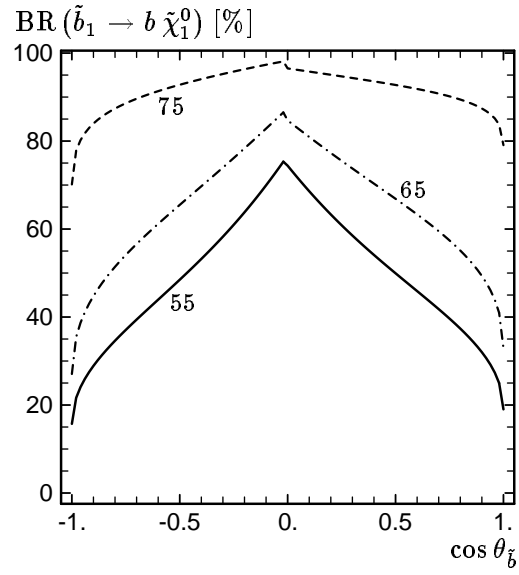


Figure 7

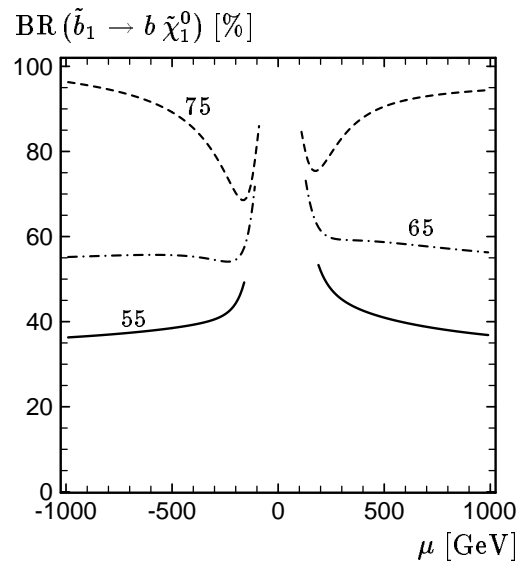


Figure 8

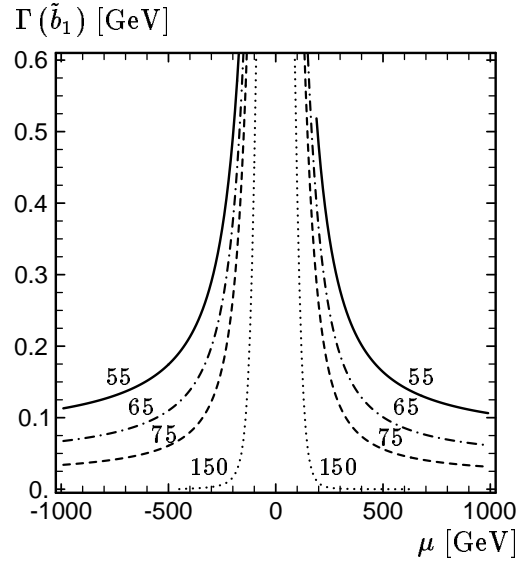


Figure 9

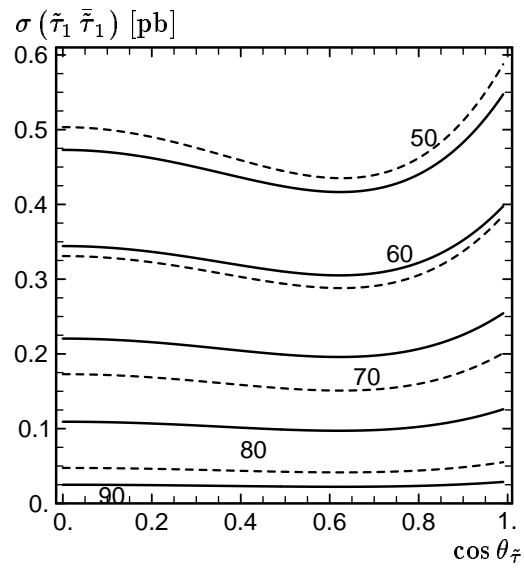


Figure 10

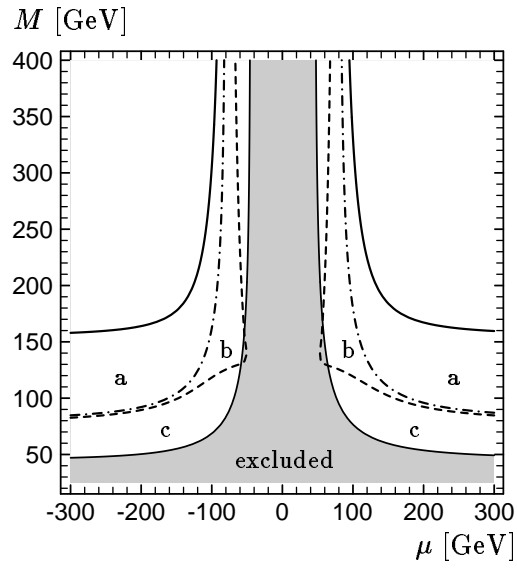


Figure 11

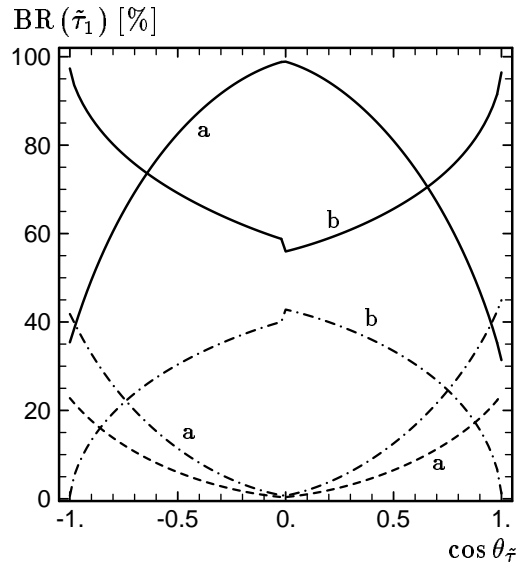


Figure 12

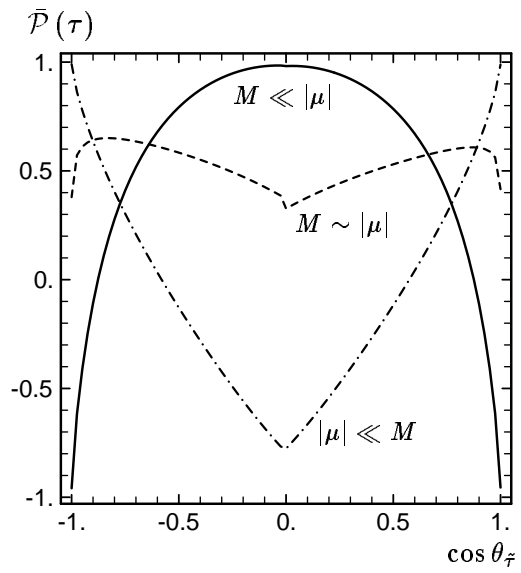


Figure 13